



First-Principles Investigation of Thermoelectric Properties of Ternary ScNiSb and Quaternary MgTiNi₂Sb₂ Half-Heusler Compounds: A Comparative Study

Tanju GÜREL^{*1}, Musa Rıza EROĞLU¹, Cem SEVİK^{2,3}

¹Department of Physics, Tekirdağ Namik Kemal University, Tekirdağ, TR-59030, Turkey

²Department of Mechanical Engineering, Eskisehir Technical University, Eskisehir, TR-26555, Turkey

³Department of Physics & NANOlaboratory Center of Excellence, University of Antwerp, Groenenborgerlaan 171, B-2020 Antwerp, Belgium

Research Article

Keywords:

first principles
 half-Heusler compounds
 thermoelectric properties

Received: 22.11.2022

Accepted: 26.12.2022

Published: 31.12.2022

DOI: 10.55848/jbst.2022.18

ABSTRACT

Ternary half-Heusler materials with 18 valence electrons show semiconducting behavior and are studied intensively because of their promising thermoelectric properties. Quaternary half-Heusler materials with four different atoms and containing 18 valence electrons, similar to their ternary counterparts, are also promising due to their low thermal conductivity. In this study, thermoelectric properties of ternary half-Heusler ScNiSb and the predicted quaternary half-Heusler MgTiNi₂Sb₂ materials are investigated from first principles. Calculations are carried out using density functional theory (DFT) within generalized gradient approximation (GGA). Equilibrium lattice parameters, bulk modulus, pressure dependence of bulk modulus, electronic band structures, total and partial electronic density of states, and vibrational properties are calculated and results are compared with available experiments and other calculations. Thermoelectric properties such as Seebeck coefficient, electrical conductivity, and electronic thermal conductivity are calculated by considering various scattering mechanisms beyond constant relaxation time approximation. Lattice thermal conductivities are calculated from phonon Boltzmann transport equation without using any experimental parameters. We have found that, by replacing the Sc atoms of ScNiSb with Mg and Ti, the obtained quaternary material MgTiNi₂Sb₂ exhibits improved *p*-type thermoelectric performance not only because of its lower thermal conductivity but also due to its enhanced electronic transport properties. We predicted the highest *p*-type $ZT=1.25$ value at 1000 K for MgTiNi₂Sb₂, which is about 2.5 times larger compared to ScNiSb. This study elucidates the promising thermoelectric performance of quaternary half-Heusler materials.

1. Introduction

In parallel with the increasing energy production, the amount of waste heat also increases. It has been predicted that the waste heat produced in 2030 will constitute approximately 50% of the global energy production [1]. Among waste heat recovery strategies, solid-state thermoelectric systems are intensively studied because they offer clean, sustainable, and environmentally friendly solution for heat-to-electricity conversion [2, 3]. The thermoelectric devices can be applied to various heat emanating systems such as sun [4] and radioisotopes [5, 6], and heat recovery systems such as transport vehicles [7], industrial systems [8, 9], and human body [10, 11]. Alternatively, the electric current applied to a thermoelectric device can also work as a solid-state heat pump which is called thermoelectric cooling [12, 13, 14]. Thermoelectric coolers are free of moving parts, silent, and suitable for miniaturization [15]. Thermoelectric modules can also be used in hybrid energy harvesting systems [16].

In order to obtain commercially efficient thermoelectric generators, the performance of thermoelectric materials must be improved by various design strategies [17, 18]. There is always room for discovery of new classes of thermoelectric materials either experimentally [19, 20, 21, 22] or computationally [23].

The efficiency of a thermoelectric material is given by a dimensionless figure of merit $ZT = S^2\sigma T/\kappa$ where S , σ , T , and κ represent the Seebeck coefficient, electrical conductivity, absolute temperature, and thermal conductivity, respectively. Here, κ is the sum of electronic (κ_e) and the lattice thermal (κ_l) conductivities. For a high value of ZT , the material must exhibit low thermal conductivity as well as high electrical conductivity

and high Seebeck coefficient. The commercial thermoelectric materials mostly have $ZT \approx 1$ but larger values of ZT are required to improve efficiency for widely usage in many different applications.

Half-Heusler compounds are promising thermoelectric materials which are intensively studied due to their high thermal stability, mechanically robustness, and excellent electrical properties [24]. These materials, containing three different elements (XYZ), are promising for high-temperature power generation applications with exhibiting $ZT \approx 1$ around 1000 K [24, 25]. One lacking property of half-Heusler materials is their relatively high lattice thermal conductivity [26] compared to well known thermoelectric materials such as Bi₂Te₃ [27] and PbTe [28]. Phonon engineering is very important in order to increase the thermoelectric efficiency of half-Heusler materials.

Recently, a new form of half-Heusler compounds has attracted attention so called quaternary or double half-Heuslers [29, 30, 31, 32, 33]. These materials are named as double half-Heuslers which are based on aliovalent substitution of XYZ with X'X''Y₂Z₂, X₂Y'Y''Z₂, or X₂Y₂Z'Z'' (where the substituted elements are not isovalent) to distinguish from other isovalently alloyed quaternary Heusler compounds [29]. Quaternary half-Heusler materials are found to exhibit lower lattice thermal conductivities compared to the half-Heusler materials, both experimentally [29, 30, 32] and computationally [29, 34]. Quaternary half-Heusler compounds are promising candidates for thermoelectric applications where low thermal conductivity is almost a must to achieve high figure of merit (ZT).

In this study, a comparative first-principles investigation

*Corresponding author: Department of Physics, Tekirdağ Namik Kemal University, Tekirdağ, TR-59030, Turkey

E-mail address: tgurel@nku.edu.tr

of half-Heusler ScNiSb and its analogue quaternary double half-Heusler (computationally predicted [29]) MgTiNi₂Sb₂ compound have been performed for their thermoelectric properties. We have found that, replacing Sc atom with Mg and Ti improves the electronic transport properties MgTiNi₂Sb₂. Together with the lower lattice thermal conductivity, its highest *p*-type *ZT* value is found as 1.25 at temperature 1000 K with a carrier concentration 10²¹ cm⁻³.

2. Computational Details

Calculations have been carried out within Vienna Ab initio Simulation Package (VASP) [35] which is based on density functional theory [36, 37]. Generalized gradient approximation (GGA) is used for describing the exchange and correlation functionals with the parameterization of Perdew-Burke-Ernzerhof (PBE) [38]. For plane waves an energy cutoff value of 500 eV was found to be converged. The convergence criteria 10⁻⁷ eV is set for self-consistent field calculations. The residual forces exerted on each atom were relaxed in the geometric optimization computations using a criteria of 10⁻² eV/Å. A converged 8 × 8 × 8 and 8 × 8 × 6 *k*-grid was employed for the total energy and geometric optimization computations for ternary and quaternary structures, respectively. A denser 21 × 21 × 21 grid for ternary and 24 × 24 × 18 grid for quaternary structures were adopted for the further calculations of the electronic density of states and thermoelectric coefficients.

Phonon dispersions and phonon density of states are calculated from second order force constants by using the PHONOPY [39] code which uses finite-differences supercell approximation. We have used a 3 × 3 × 3 supercell for both ScNiSb and MgTiNi₂Sb₂. The *k*-grids used in the phonon supercell calculations are 4 × 4 × 4 for ScNiSb and 3 × 3 × 3 for MgTiNi₂Sb₂.

Electronic transport properties are calculated beyond constant relaxation time approximation within the AMSET code [40]. Here, the scattering rates (and hence relaxation times) are obtained by considering acoustic deformation potential (ADP), ionized impurity scattering (IMP), polar optical phonon (POP), and piezoelectric (PIE) scattering processes.

We have also calculated the lattice thermal conductivity (LTC) by solving the linearized phonon Boltzmann transport equation which was implemented in the ShengBTE code [41]. Third order force constants are obtained with the help of the thirdorder.py [41] script by considering the interactions between fourth nearest neighbors. For third order force constants, we have used a 4 × 4 × 4 supercell for ScNiSb and 3 × 3 × 3 for MgTiNi₂Sb₂. For both materials, the *k*-grid for the supercells is set to single Γ -point. In the ShengBTE calculations, we have used a converged *q*-grid 24 × 24 × 24 for ScNiSb and 16 × 16 × 12 for MgTiNi₂Sb₂. The scalebroad factor is set to 1.0 for all calculations.

3. Results

3.1. Structural properties

Ternary half-Heusler ScNiSb material crystallize in face-centered cubic structure and belongs to the space group $F\bar{4}3m$ (group no. 216). The primitive cell of the structure contains three atoms, one for Sc, one for Ni, and one for Sb. When we add another primitive cell to the primitive cell of the face-centered cubic structure of the ternary half-Heusler ScNiSb in a chosen direction (*z* direction is preferred in this study), the new structure contains two Sc, two Ni and, two Sb atoms. When we replace the two Sc atoms with Mg and Ti, the new MgTiNi₂Sb₂ material is formed. As a result of these atomic exchanges, the crystal symmetry changes. The Ni atoms move slightly away from

Table 1. Lattice parameters, bulk modulus, and the pressure derivative of the bulk modulus of ScNiSb and MgTiNi₂Sb₂

Material	Study	<i>a</i> (Å)	<i>c</i> (Å)	<i>B</i> ₀ (GPa)	<i>B</i> '
ScNiSb	This Work	6.108		105.71	4.56
	Calc.[43]	6.104		105.030	4.57
	Calc.[44]	6.055			
	Calc.[45]	6.138		106.03	
	Expt.[46]	6.068(2)			
MgTiNi ₂ Sb ₂	This Work	4.251	6.003	104.20	4.65

their cubic symmetry position in the *z*-direction and the system becomes tetragonal. The resulting MgTiNi₂Sb₂ quaternary double half-Heusler material crystallizes in the space group $P\bar{4}m2$ (group no. 115) [34, 42].

The optimized lattice parameters, bulk modulus, and the pressure derivative of the bulk modulus of ScNiSb and MgTiNi₂Sb₂ are presented in Table 1 along with available experiments and other calculations. Our calculated results of ScNiSb are in best agreement with the computational study of Kocak and Ciftci [43]. The calculated lattice parameter of ScNiSb is slightly (0.7%) larger than experimental measurement [46] which is a typical behavior of GGA functional. The bulk modulus and its pressure derivative are calculated by using Birch-Murnaghan equation of state [47, 48]. We found that there is no meaningful difference of bulk modulus and its pressure derivative between ScNiSb and MgTiNi₂Sb₂. Our calculated bulk modulus of ScNiSb is in good agreement with the previous studies of Refs. [43] and [45].

3.2. Phonon dispersions and phonon density of states.

The phonon dispersion curves obtained by the direct method are given in Fig. 1 for ScNiSb and in Fig. 2 for MgTiNi₂Sb₂. The ternary half-Heusler material ScNiSb has three atoms in the primitive cell and therefore has nine vibrational modes, three acoustic and six optical. The quaternary half-Heusler structure of MgTiNi₂Sb₂ has 18 vibrational modes, three acoustic and 15 optical, since there are six atoms in its primitive cell. The positive phonon frequencies in all modes indicate that the materials are dynamically stable. In ScNiSb material, there is a frequency gap around 4.5-5 THz between acoustic and optical modes. For MgTiNi₂Sb₂, hybridization between the low optical and acoustic modes is observed around 3 THz and there exist avoided crossings between the acoustic modes and the lowest optical modes in the $\Gamma - X$ and $R - A$ paths. The hybridization and these avoided crossings appear to be one of the important factors that reduce the thermal conductivity of the lattice [49, 50].

The calculated phonon density of states for ScNiSb and MgTiNi₂Sb₂ are given in Figs. 3 and 4, respectively. In general, in both materials, antimony atoms contribute predominantly to the acoustic modes. In the case of MgTiNi₂Sb₂, Sb atoms also contribute predominantly in the low optical modes that hybridize with the acoustic modes. For ScNiSb, the low optical modes between 5-6 THz contain mainly Ni atoms and the high optical modes between 6.5-7.5 THz contain mainly Sc atoms. For MgTiNi₂Sb₂ material, Ti and Ni atoms contribute at 4.5-7.5 THz and Mg atoms contribute at 7.5-8.5 THz in the 4.5-8.5 THz optical frequency region.

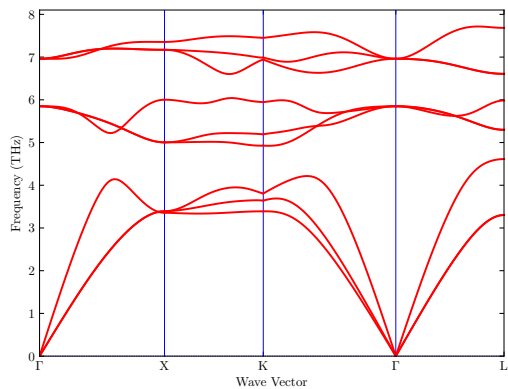


Fig. 1. Phonon dispersion relations of half-Heusler ScNiSb.

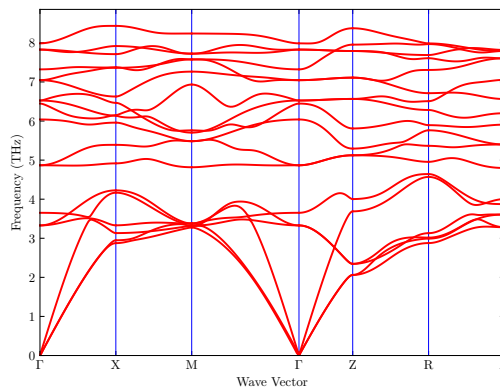


Fig. 2. Phonon dispersion relations of quaternary double half-Heusler MgTiNi₂Sb₂.

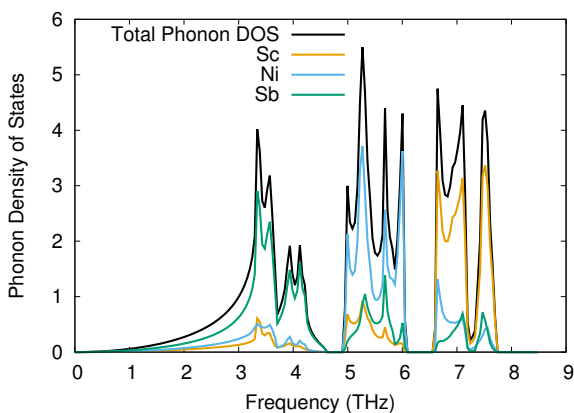


Fig. 3. Phonon density of states of ScNiSb.

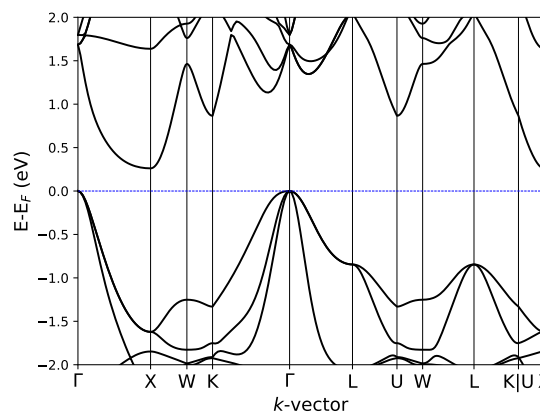


Fig. 5. Electronic band structure of ScNiSb.

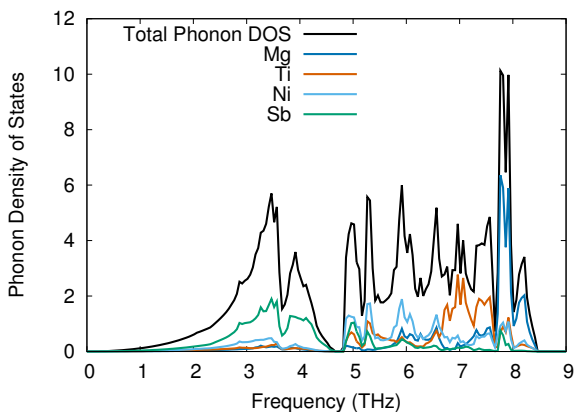


Fig. 4. Phonon density of states of MgTiNi₂Sb₂.

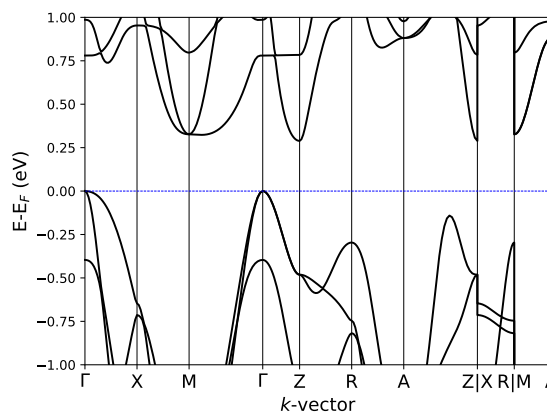


Fig. 6. Electronic band structure of MgTiNi₂Sb₂.

3.3. Electronic properties

Electronic band structures of ScNiSb and MgTiNi₂Sb₂ are shown in Figs. 5 and 6, respectively. Both materials exhibit indirect band gap. The GGA-PBE indirect band gap of ScNiSb between $\Gamma - X$ points of the Brillouin zone is calculated as 0.26 eV. This band gap value is surprisingly very close to the experimental result 0.259 eV of Ref. [51]. This agreement should be denoted as accidental, because it is well known that GGA band gaps mostly underestimate experimental measurements. As also stated in Refs. [51] and [52], the experimental band gaps strongly influenced by the crystallographic disorder. The indirect band gap

of MgTiNi₂Sb₂ is found slightly larger with 0.29 eV between the points $\Gamma - Z$.

Electronic total and partial density of states are presented in Figs. 7 and 8 for ScNiSb and MgTiNi₂Sb₂, respectively. As shown in Fig. 7, the main contributions near valence band of Fermi level mostly come from Sc *d*-states compared to Ni and Sb atoms. For MgTiNi₂Sb₂ in Fig. 8, both valence region and conduction region exhibit very different behavior when we replace the Sc atoms with Mg and Ti. The magnesium *s*-states have large contributions to the

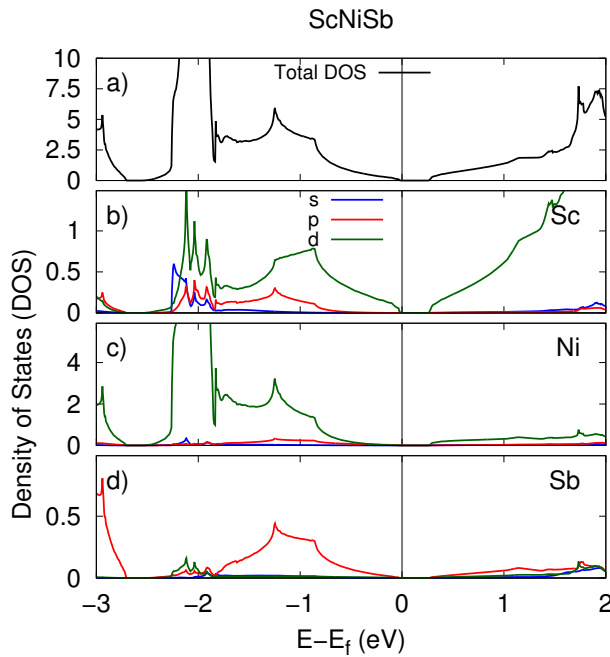


Fig. 7. Total and partial electronic density of states of ScNiSb.

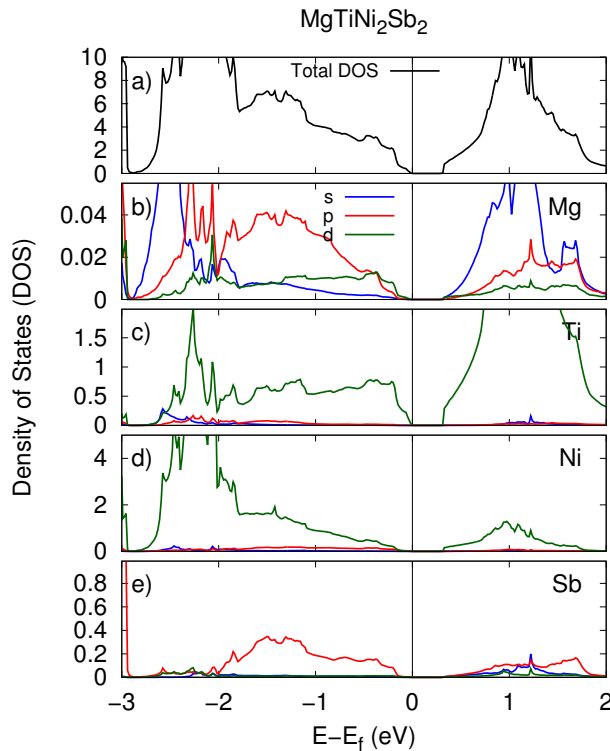


Fig. 8. Total and partial electronic density of states of MgTiNi₂Sb₂.

conduction bands and the titanium atoms have large contributions to the valence bands with a sharp slope near Fermi level. This slope is an indication of large *p*-type Seebeck coefficients [53, 54]. In the case of ScNiSb, this slope is not observed.

3.4. Thermoelectric properties

Electronic transport properties, such as Seebeck coefficients, electrical conductivity, and electronic thermal conductivity are given in Fig. 9 as a function of carrier concentration for both electron (*n*-type) and hole (*p*-type) dopings in a temperature range of 300-1000 K. The materials parameters, required to obtain

scattering rates and hence electronic transport properties, such as elastic constants, deformation potentials, static and high-frequency dielectric constants, wave-function coefficients, and polar-phonon frequency are calculated within DFT and density functional perturbation theory (DFPT) [55].

The Seebeck coefficients are given in Figs. 9(a) and 9(d) for *p*-type and *n*-type systems, respectively. Since the band gaps of both materials are relatively narrow, the bipolar conduction effect causes dramatic decrease in Seebeck coefficients at high temperatures and low concentrations for both *p*-type and *n*-type dopings. The atomic replacement of Sc with Mg and Ti results a large increase in Seebeck coefficients for *p*-type doping, particularly at concentrations around 10^{21} cm^{-3} . For the *n*-type doping, Seebeck coefficients of MgTiNi₂Sb₂ slightly lower than ScNiSb around around 10^{21} cm^{-3} concentrations.

Figs. 9(b) and 9(e) presents the electrical conductivity of ScNiSb and MgTiNi₂Sb₂ for *p*-type and *n*-type dopings, respectively. As can be seen from figures, electrical conductivity decreases (increases) with increasing temperature (carrier concentration) for both doping types. The effect of atomic replacement from ScNiSb to MgTiNi₂Sb₂ is found to be small for *p*-type doping. But for the *n*-type doping, this replacement caused a large decrement, especially at higher concentrations.

In Figs. 9(c) and 9(f), we present electronic thermal conductivity of ScNiSb and MgTiNi₂Sb₂ for *p*-type and *n*-type dopings, respectively. For the *p*-type electronic thermal conductivity, the difference between two materials is relatively small. But for the *n*-type doping, a large decrement is observed with the replacement of Sc with Mg and Ti starting from 10^{21} cm^{-3} to higher concentrations.

Before discussing the power factors and the *ZT* values, we discuss the phonon transport properties of ScNiSb and MgTiNi₂Sb₂. We present our calculated lattice thermal conductivity results in Fig. 10 which was obtained from the phonon Boltzmann transport equation without using any empirical parameters. As shown in figure, the calculated ScNiSb lattice thermal conductivity is in a very good with experimental measurements from 300 to 600 K. The increase of experimental thermal conductivity after 600 K is attributed to the possible heat losses during the measurements and contributions from bipolar effects [56]. Since the structure of MgTiNi₂Sb₂ is tetragonal, we have found a small anisotropy where the LTC in *z*-direction is slightly lower than *x*- and *y*-directions. The average lattice thermal conductivity of MgTiNi₂Sb₂ is calculated to be about 25% lower than ScNiSb which is important to obtain larger *ZT* values.

The calculated Mode Grüneisen parameters, phonon group velocities, and anharmonic scattering rates are given in Fig. 11. The overall mode Grüneisen parameters for both materials are positive and between 0.5 and 2.2 values as shown in Fig. 11(a). In Fig. 11(b), the phonon group velocities of MgTiNi₂Sb₂ at acoustic region (0-4 THz) are considerably lower than those of ScNiSb which is an indication of lower thermal conductivity as we reported in Fig. 10. Similar behavior is also reported in TiCoSb and Ti₂FeNiSb₂ systems [29]. The anharmonic scattering rates presented in Fig. 11(b) have found to be similar for both materials.

The calculated power factors ($\text{PF} = S^2 \sigma$) and the *ZT* values are given in Fig. 12 as a function of carrier concentration for *n*-type and *p*-type dopings in a temperature range of 300-1000 K. Due to the higher *p*-type Seebeck coefficients of MgTiNi₂Sb₂, the highest power factors are almost two times larger compared to ScNiSb (Fig. 12(a)). We obtained highest PFs of MgTiNi₂Sb₂ at carrier concentrations around $2 \times 10^{21} \text{ cm}^{-3}$. In the *n*-type doping, lower electrical conductivity of MgTiNi₂Sb₂ strongly effects to the PF and the highest PFs are found about half of value compared to

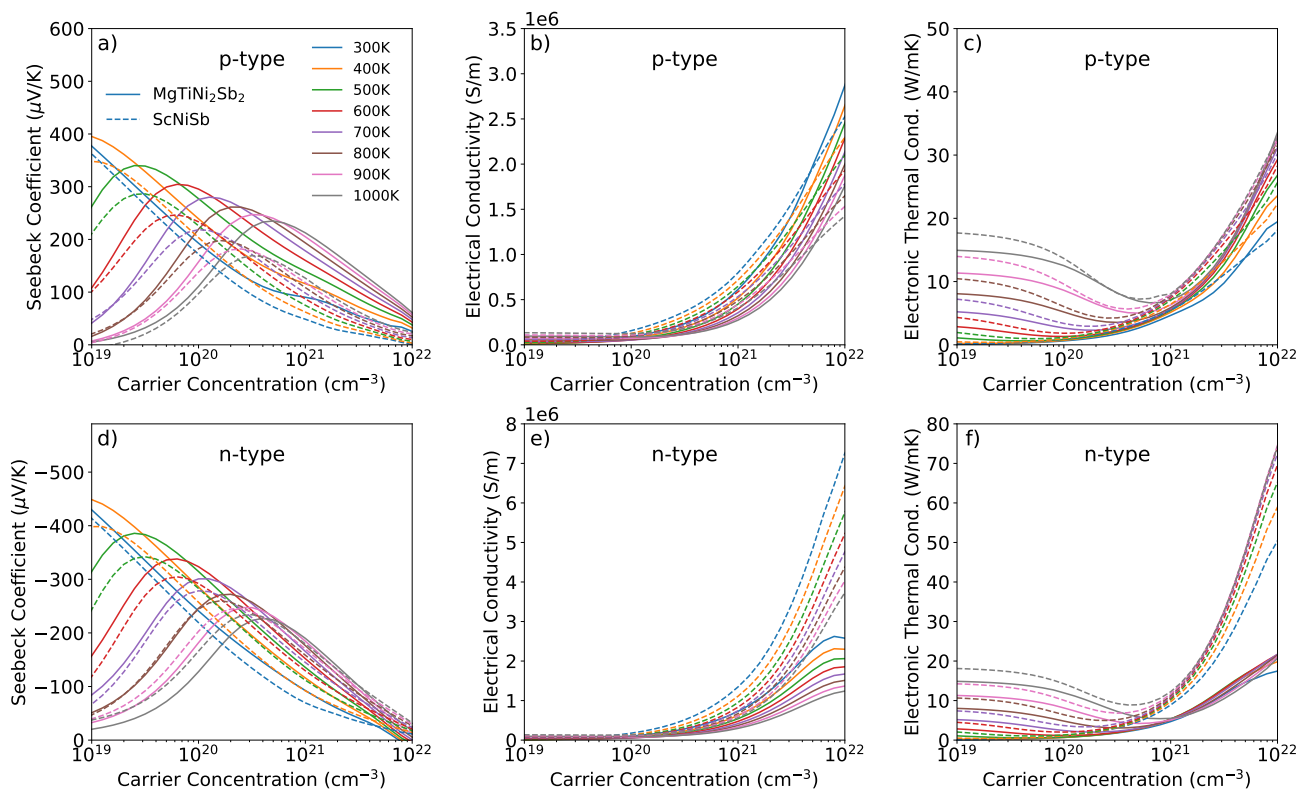


Fig. 9. Electronic transport properties of ScNiSb (dashed lines) and MgTiNi₂Sb₂ (full lines) as a function of carrier concentration with temperatures in the range of 300–1000 K. (a) Seebeck coefficient, (b) electrical conductivity, and (c) electronic thermal conductivity for *p*-type doping; and (d) Seebeck coefficient, (e) electrical conductivity, and (f) electronic thermal conductivity for *n*-type system.

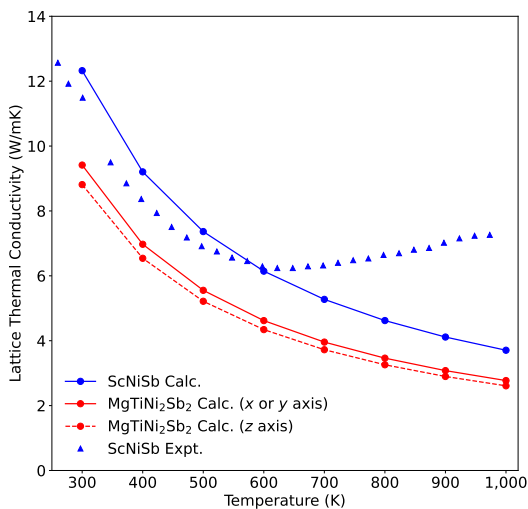


Fig. 10. Lattice thermal conductivity of ScNiSb and MgTiNi₂Sb₂. Experimental values are taken from Ref. [56]

ScNiSb (Fig. 12(c)).

Finally, the calculated *ZT* values of ScNiSb and MgTiNi₂Sb₂ as a function of carrier concentration in a temperature range of 300-1000 K for *n*-type and *p*-type dopings are given in Fig. 12(b) and Fig. 12(d), respectively. The total thermal conductivity, as a sum of calculated lattice and electronic thermal conductivities, is used for obtaining *ZT* values. For both materials, the optimum *ZT* values at each temperature varies with carrier concentration.

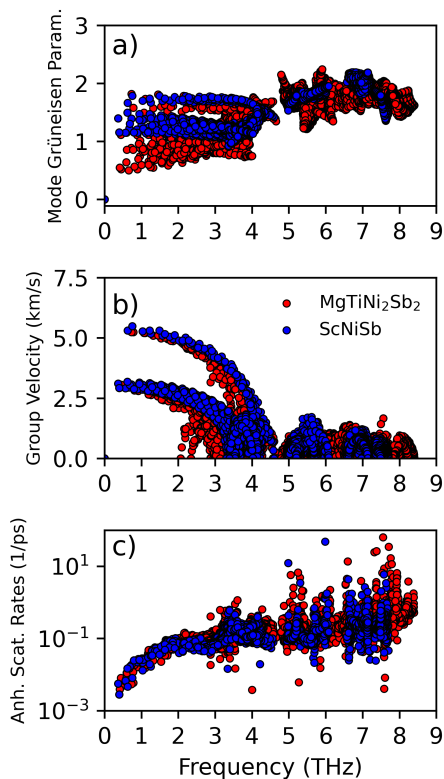


Fig. 11. (a) Mode Grüneisen parameters, (b) phonon group velocities, and (c) anharmonic scattering rates of ScNiSb (red dots) and MgTiNi₂Sb₂ (blue dots).

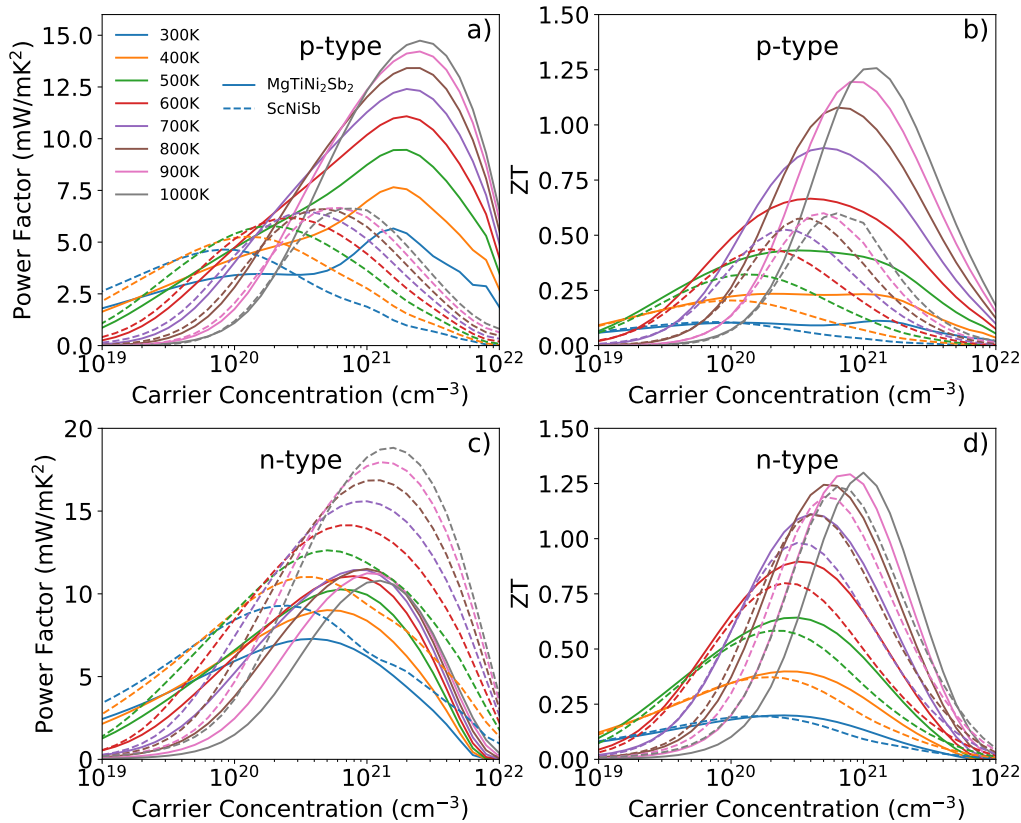


Fig. 12. Power factor and ZT of ScNiSb (dashed lines) and MgTiNi₂Sb₂ (full lines) as a function of carrier concentration with temperatures in the range of 300–1000 K. (a) Power factor and (b) ZT of the p -type doping, and (c) power factor and (d) ZT of the n -type doping.

The highest p -type ZT values for ScNiSb is found to be around 0.5 in a temperature range of 700-1000 K. But for MgTiNi₂Sb₂, the highest p -type ZT values continue to increase with respect temperature and reach to $ZT=1.25$ value at 1000 K at a carrier concentration of 10^{21} cm⁻³. Thus, by replacing of Sc atoms with Mg and Ti, we achieved an 2.5 fold increase in ZT for p -type doping. For n -type doping, the ZT values are found similar for both materials where the highest ZT is obtained about 1.25 at carrier concentration around 10^{21} cm⁻³.

4. Conclusion

In this study, a comparative investigation of the thermoelectric properties of the ternary half-Heusler ScNiSb and quaternary double half-Heusler MgTiNi₂Sb₂ have been performed from first principles. We have found that lattice thermal conductivity of MgTiNi₂Sb₂ is about 25% lower than ScNiSb which is valuable for higher thermoelectric performance. More importantly, replacement of Sc atoms with Mg and Ti atoms improved the electronic transport properties and hence power factors and ZT values for p -type system. We have predicted the highest p -type $ZT=1.25$ value of MgTiNi₂Sb₂ at 1000 K which is about 2.5 times larger than the ZT value of ScNiSb at the same temperature. Thus, from our calculations, we conclude that the quaternary half-Heusler materials are promising novel thermoelectric materials worth further synthesizing efforts, not only for their lower thermal conductivity behavior, but also for their enhanced electronic transport properties.

Declaration

Author Contribution: Conceive-T.G.; Design-T.G.; Supervision-T.G.; Computational Performance, Data Collection and/or Processing-T.G., M.R.E.; Analysis and/or Interpretation Literature Review-T.G., M.R.E., C.S.; Writer-T.G.; Critical Reviews-T.G., C.S.;

Acknowledgment: The numerical calculations reported in this paper were partially performed at TUBITAK ULAKBIM, High Performance and Grid Computing Center (TRUBA resources).

Conflict of Interest: The authors have declared no conflicts of interest.

Orcid ID:

Tanju GÜREL 0000-0002-2623-5081

Musa Rıza EROĞLU 0000-0002-7390-580X

Cem SEVİK 0000-0002-2412-9672

References

- [1] A. Firth, B. Zhang, and A. Yang. "Quantification of global waste heat and its environmental effects". *Applied Energy* 235 (2019), pp. 1314–1334. DOI: 10.1016/j.apenergy.2018.10.102.

- [2] L. E. Bell. "Cooling, Heating, Generating Power, and Recovering Waste Heat with Thermoelectric Systems". *Science* 321 (2008), pp. 1457–1461. DOI: 10.1126/science.1158899.
- [3] D. Champier. "Thermoelectric generators: A review of applications". *Energy Conversion and Management* 140 (2017), pp. 167–181. DOI: 10.1016/j.enconman.2017.02.070.
- [4] L. C. Ding, A. Akbarzadeh, and L. Tan. "A review of power generation with thermoelectric system and its alternative with solar ponds". *Renewable and sustainable energy reviews* 81 (2018), pp. 799–812. DOI: 10.1016/j.rser.2017.08.010.
- [5] J. Yang and T. Caillat. "Thermoelectric materials for space and automotive power generation". *MRS bulletin* 31 (2006), pp. 224–229.
- [6] R. M. Ambrosi et al. "European radioisotope thermoelectric generators (RTGs) and radioisotope heater units (RHUs) for space science and exploration". *Space Science Reviews* 215 (2019), pp. 1–41. DOI: 10.1007/s11214-019-0623-9.
- [7] B. Orr, A. Akbarzadeh, M. Mochizuki, and R. Singh. "A review of car waste heat recovery systems utilising thermoelectric generators and heat pipes". *Applied thermal engineering* 101 (2016), pp. 490–495. DOI: 10.1016/j.applthermaleng.2015.10.081.
- [8] S. Hooshmand Zaferani, M. Jafarian, D. Vashae, and R. Ghomashchi. "Thermal Management Systems and Waste Heat Recycling by Thermoelectric Generators—An Overview". *Energies* 14 (2021), p. 5646. DOI: 10.3390/en14185646.
- [9] H. Jouhara, N. Khordehgah, S. Almahmoud, B. Delpech, A. Chauhan, and S. A. Tassou. "Waste heat recovery technologies and applications". *Thermal Science and Engineering Progress* 6 (2018), pp. 268–289. DOI: 10.1016/j.tsep.2018.04.017.
- [10] A. R. M. Siddique, S. Mahmud, and B. Van Heyst. "A review of the state of the science on wearable thermoelectric power generators (TEGs) and their existing challenges". *Renewable and Sustainable Energy Reviews* 73 (2017), pp. 730–744. DOI: 10.1016/j.rser.2017.01.177.
- [11] C. Yang et al. "Transparent flexible thermoelectric material based on non-toxic earth-abundant p-type copper iodide thin film". *Nature communications* 8 (2017), Article 16076. DOI: 10.1038/ncomms16076.
- [12] F. J. DiSalvo. "Thermoelectric cooling and power generation". *Science* 285 (1999), pp. 703–706. DOI: 10.1126/science.285.5428.703.
- [13] D. Zhao and G. Tan. "A review of thermoelectric cooling: materials, modeling and applications". *Applied thermal engineering* 66 (2014), pp. 15–24. DOI: 10.1016/j.applthermaleng.2014.01.074.
- [14] J. Mao, G. Chen, and Z. Ren. "Thermoelectric cooling materials". *Nature Materials* 20 (2021), pp. 454–461. DOI: 10.1038/s41563-020-00852-w.
- [15] R. A. Kishore, A. Nozariasbmarz, B. Poudel, M. Sanghadasa, and S. Priya. "Ultra-high performance wearable thermoelectric coolers with less materials". *Nature communications* 10 (2019), Article 1765. DOI: 10.1038/s41467-019-09707-8.
- [16] H. Ryu, H.-J. Yoon, and S.-W. Kim. "Hybrid energy harvesters: toward sustainable energy harvesting". *Advanced Materials* 31 (2019), Article 1802898. DOI: 10.1002/adma.201802898.
- [17] G. Tan, L.-D. Zhao, and M. G. Kanatzidis. "Rationally Designing High-Performance Bulk Thermoelectric Materials". *Chemical Reviews* 116 (2016). PMID: 27580481, pp. 12123–12149. DOI: 10.1021/acs.chemrev.6b00255.
- [18] J. He and T. M. Tritt. "Advances in thermoelectric materials research: Looking back and moving forward". *Science* 357 (2017), eaak9997. DOI: 10.1126/science.aak9997.
- [19] M. G. Kanatzidis. "The role of solid-state chemistry in the discovery of new thermoelectric materials". *semiconductors and semimetals*. Vol. 69. Elsevier, 2001, pp. 51–100. DOI: 10.1016/S0080-8784(01)80149-6.
- [20] D.-Y. Chung, T. P. Hogan, M. Rocci-Lane, P. Brazis, J. R. Ireland, C. R. Kannewurf, M. Bastea, C. Uher, and M. G. Kanatzidis. "A new thermoelectric material: CsBi₄Te₆". *Journal of the American Chemical Society* 126 (2004), pp. 6414–6428. DOI: 10.1021/ja039885f.
- [21] L.-D. Zhao, S.-H. Lo, Y. Zhang, H. Sun, G. Tan, C. Uher, C. Wolverton, V. P. Dravid, and M. G. Kanatzidis. "Ultralow thermal conductivity and high thermoelectric figure of merit in SnSe crystals". *Nature* 508 (2014), pp. 373–377. DOI: 10.1038/nature13184.
- [22] J. Zhang, L. Song, S. H. Pedersen, H. Yin, L. T. Hung, and B. B. Iversen. "Discovery of high-performance low-cost n-type Mg₃Sb₂-based thermoelectric materials with multi-valley conduction bands". *Nature communications* 8 (2017), Article 13901. DOI: 10.1038/ncomms13901.
- [23] P. Gorai, V. Stevanović, and E. S. Toberer. "Computationally guided discovery of thermoelectric materials". *Nature Reviews Materials* 2 (2017), Article 17053. DOI: 10.1038/natrevmats.2017.53.
- [24] T. Zhu, C. Fu, H. Xie, Y. Liu, and X. Zhao. "High efficiency half-Heusler thermoelectric materials for energy harvesting". *Advanced Energy Materials* 5 (2015), p. 1500588. DOI: 10.1002/aenm.201500588.
- [25] R. J. Quinn and J.-W. G. Bos. "Advances in half-Heusler alloys for thermoelectric power generation". *Mater. Adv.* 2 (2021), pp. 6246–6266. DOI: 10.1039/D1MA00707F.
- [26] W. Ren, X. Shi, Z. Wang, and Z. Ren. "Crystallographic design for half-Heuslers with low lattice thermal conductivity". *Materials Today Physics* 25 (2022), Article 100704. DOI: 10.1016/j.mtphys.2022.100704.

- [27] I. T. Witting, T. C. Chasapis, F. Ricci, M. Peters, N. A. Heinz, G. Hautier, and G. J. Snyder. "The thermoelectric properties of bismuth telluride". *Advanced Electronic Materials* 5 (2019), p. 1800904. DOI: 10.1002/aelm.201800904.
- [28] Z. Tian, J. Garg, K. Esfarjani, T. Shiga, J. Shiomi, and G. Chen. "Phonon conduction in PbSe, PbTe, and PbTe_{1-x}Se_x from first-principles calculations". *Phys. Rev. B* 85 (2012), p. 184303. DOI: 10.1103/PhysRevB.85.184303.
- [29] S. Anand, M. Wood, Y. Xia, C. Wolverton, and G. J. Snyder. "Double Half-Heuslers". *Joule* 3 (2019), pp. 1226–1238. DOI: 10.1016/j.joule.2019.04.003.
- [30] "Design of High-Performance Disordered Half-Heusler Thermoelectric Materials Using 18-Electron Rule". *Adv. Funct. Mater.* 29 (2019), p. 1905044. DOI: 10.1002/adfm.201905044.
- [31] A. Horyn, O. Bodak, L. Romaka, Y. Gorelenko, A. Tkachuk, V. Davydov, and Y. Stadnyk. "Crystal structure and physical properties of (Ti, Sc)NiSn and (Zr, Sc)NiSn solid solutions". *J. Alloys Compd.* 363 (2004), pp. 10–14. DOI: 10.1016/S0925-8388(03)00448-1.
- [32] Q. Wang et al. "Enhanced Thermoelectric Properties in p-Type Double Half-Heusler Ti₂-yHf_yFeNiSb₂-xSn_x Compounds". *Phys. Status Solidi Appl. Mater. Sci.* 217 (2020), pp. 2–8. DOI: 10.1002/pssa.202000096.
- [33] J. Tobała, L. Jodin, P. Pecher, H. Scherrer, G. Venturini, B. Malaman, and S. Kaprzyk. "Composition-induced metal-semiconductor-metal crossover in half-Heusler Fe_{1-x}Ni_xTiSb". *Phys. Rev. B - Condens. Matter Mater. Phys.* 64 (2001), pp. 1551031–1551037. DOI: 10.1103/PhysRevB.64.155103.
- [34] M. K. Choudhary and P. Ravindran. "Thermal, electronic and thermoelectric properties of TiNiSn and TiCoSb based quaternary half Heusler alloys obtained from: Ab initio calculations". *Sustain. Energy Fuels* 4 (2020), pp. 895–910. DOI: 10.1039/c9se01047e.
- [35] G. Kresse and J. Furthmüller. "Efficient iterative schemes for ab initio total-energy calculations using a plane-wave basis set". *Phys. Rev. B* 54 (1996), pp. 11169–11186. DOI: 10.1103/PhysRevB.54.11169.
- [36] P. Hohenberg and W. Kohn. "Inhomogeneous Electron Gas". *Phys. Rev.* 136 (1964), B864–B871. DOI: 10.1103/PhysRev.136.B864.
- [37] W. Kohn and L. J. Sham. "Self-Consistent Equations Including Exchange and Correlation Effects". *Phys. Rev.* 140 (1965), A1133–A1138. DOI: 10.1103/PhysRev.140.A1133.
- [38] J. P. Perdew, K. Burke, and M. Ernzerhof. "Generalized Gradient Approximation Made Simple". *Phys. Rev. Lett.* 77 (1996), pp. 3865–3868. DOI: 10.1103/PhysRevLett.77.3865.
- [39] A. Togo and I. Tanaka. "First principles phonon calculations in materials science". *Scr. Mater.* 108 (2015), pp. 1–5. DOI: 10.1016/j.scriptamat.2015.07.021.
- [40] A. M. Ganose, J. Park, A. Faghaninia, R. Woods-Robinson, K. A. Persson, and A. Jain. "Efficient calculation of carrier scattering rates from first principles". *Nature communications* 12 (2021), Article 2222. DOI: 10.1038/s41467-021-22440-5.
- [41] W. Li, J. Carrete, N. A. Katcho, and N. Mingo. "ShengBTE: A solver of the Boltzmann transport equation for phonons". *Comput. Phys. Commun.* 185 (2014), pp. 1747–1758. DOI: 10.1016/j.cpc.2014.02.015.
- [42] L. Chaput, J. Tobola, P. Pécheur, and H. Scherrer. "Electronic structure and thermopower of Ni(Ti_{0.5}Hf_{0.5})Sn and related half-Heusler phases". *Phys. Rev. B* 73 (2006), Article 045121. DOI: 10.1103/PhysRevB.73.045121.
- [43] B. Kocak and Y. O. Ciftci. "The effect of pressure on structural, electronic, elastic, vibration and optical properties of ScXSb (X=Ni, Pd, Pt) compounds". *Computational Condensed Matter* 14 (2018), pp. 176–185. DOI: 10.1016/j.cocom.2018.01.009.
- [44] S. D. Guo. "Importance of spin-orbit coupling in power factor calculations for half-Heusler ANiB (A = Ti, Hf, Sc, Y; B=Sn, Sb, Bi)". *Journal of Alloys and Compounds* 663 (2016), pp. 128–133. DOI: 10.1016/j.jallcom.2015.12.139.
- [45] M. J. Winiarski, K. Bilińska, K. Ciesielski, and D. Kaczorowski. "Thermoelectric performance of p-type half-Heusler alloys ScMSb (M = Ni, Pd, Pt) by ab initio calculations". *Journal of Alloys and Compounds* 762 (2018), pp. 901–905. DOI: 10.1016/j.jallcom.2018.05.257.
- [46] T. Harmening, H. Eckert, and R. Pöttgen. "Defects in half-Heusler type antimonides ScTSb (T = Ni, Pd, Pt)". *Solid State Sciences* 11 (2009), pp. 900–906. DOI: 10.1016/j.solidstatesciences.2008.12.007.
- [47] P. Bulut, B. Beceren, S. Yıldırım, C. Sevik, and T. Gürel. "Promising room temperature thermoelectric conversion efficiency of zinc-blende AgI from first principles". *J. Phys. Condens. Matter* 33 (2021), p. 015501. DOI: 10.1088/1361-648X/abb867.
- [48] M. Hebbache and M. Zemzemi. "Ab initio study of high-pressure behavior of a low compressibility metal and a hard material: Osmium and diamond". *Phys. Rev. B* 70 (2004), p. 224107. DOI: 10.1103/PhysRevB.70.224107.
- [49] W. Li, J. Carrete, G. K. Madsen, and N. Mingo. "Influence of the optical-acoustic phonon hybridization on phonon scattering and thermal conductivity". *Phys. Rev. B* 93 (2016), p. 205203. DOI: 10.1103/PhysRevB.93.205203.

- [50] R. L. González-Romero, A. Antonelli, A. S. Chaves, and J. J. Meléndez. “Ultralow and anisotropic thermal conductivity in semiconductor As_2Se_3 ”. *Phys. Chem. Chem. Phys.* 20 (2018), pp. 1809–1816. DOI: 10.1039/c7cp07242b.
- [51] K. Ciesielski, K. Synoradzki, I. Wolanska, P. Stachowiak, L. Kepinski, A. Jezowski, T. Tolinski, and D. Kaczorowski. “High-temperature power factor of half-Heusler phases RENiSb (RE = Sc, Dy, Ho, Er, Tm, Lu)”. *Journal of Alloys and Compounds* 816 (2020), p. 152596. DOI: 10.1016/j.jallcom.2019.152596.
- [52] K. Ciesielski, I. Wolańska, K. Synoradzki, D. Szymański, and D. Kaczorowski. “Mobility Ratio as a Probe for Guiding Discovery of Thermoelectric Materials: The Case of Half-Heusler Phase $\text{ScNiSb}_{1-x}\text{Te}_x$ ”. *Phys. Rev. Applied* 15 (2021), p. 044047. DOI: 10.1103/PhysRevApplied.15.044047.
- [53] G. Sun, Y. Li, X. Zhao, Y. Mi, and L. Wang. “First-Principles Investigation of the Effect of M-Doped (M = Zr, Hf) TiCoSb Half-Heusler Thermoelectric Material”. *J. Mater. Sci. Chem. Eng.* 03 (2015), pp. 78–86. DOI: 10.4236/msce.2015.312012.
- [54] A. N. Gandi and U. Schwingenschlögl. “Thermoelectric Properties of the XCoSb (X: Ti,Zr,Hf) Half-Heusler alloys”. *Phys. Status Solidi Basic Res.* 254 (2017), p. 1700419. DOI: 10.1002/pssb.201700419.
- [55] S. Baroni, S. de Gironcoli, A. Dal Corso, and P. Giannozzi. “Phonons and related crystal properties from density-functional perturbation theory”. *Rev. Mod. Phys.* 73 (2001), pp. 515–562. DOI: 10.1103/RevModPhys.73.515.
- [56] K. Synoradzki, K. Ciesielski, I. Veremchuk, H. Borrmann, P. Skokowski, D. Szymański, Y. Grin, and D. Kaczorowski. “Thermal and Electronic Transport Properties of the Half-Heusler Phase ScNiSb ”. *Materials* 12 (2019). DOI: 10.3390/ma12101723.